

Physics-Informed Evidential Network: A General Framework for Uncertainty Evaluation in Nonlinear Dynamic Measurement Systems

Wenhao Chen^{ID}, Yinye Ding^{ID}, Rencheng Song^{ID}, Senior Member, IEEE, Chengliang Pan^{ID}, Huining Zhao^{ID}, Hongli Li^{ID}, and Haojie Xia^{ID}, Member, IEEE

Abstract—The application of dynamic systems in modern industrial measurement is becoming increasingly prevalent, making the credibility analysis of their measurement results critically important. However, current uncertainty evaluation methods face significant challenges when dealing with nonlinear systems. To address this challenge, we propose a physics-informed evidential network (PIENet) framework. This approach integrates governing differential equations with measurement data to impose physical constraints and guide the modeling of unknown system components, thereby enhancing predictive accuracy and robustness. It further introduces deep evidential regression and combines the uncertainty-aware loss function with physical constraints to enhance the model calibration capability and enable efficient quantification of prediction uncertainty. We further validate our proposed method on experimental datasets of nonlinear dynamic systems, and the results demonstrate that the method effectively models system dynamics and provides reliable uncertainty predictions, even in the presence of missing variables in the system equations. This approach makes a significant contribution to the use of deep learning (DL) for evaluating uncertainty in dynamic systems, which is crucial for enhancing the reliability of measurements.

Index Terms—Deep learning (DL), evidential network (ENet), nonlinear dynamic system, physical information, uncertainty evaluation.

I. INTRODUCTION

IN MODERN instrumentation and measurement (I&M) field, as the significance of dynamic measurements continues to grow, evaluating the uncertainty of dynamic measurement systems has emerged as a critical scientific issue in the field of metrology [1], [2], [3]. In many nonlinear dynamic systems, analytical uncertainty propagation is difficult to formulate or may be infeasible due to model complexity and nonlinearity, which motivates computational approaches that complement the traditional guide to the expression of uncertainty in measurement (GUM)-based evaluation [4], [5].

Received 16 August 2025; revised 24 October 2025; accepted 20 November 2025. Date of publication 11 December 2025; date of current version 18 December 2025. This work was supported in part by the National Key Research and Development Program of China under Grant 2023YFF0719700 and in part by the National Natural Science Foundation of China under Grant 52575620. The Associate Editor coordinating the review process was Dr. Anant Kumar Verma. (Corresponding author: Haojie Xia.)

The authors are with Anhui Province Key Laboratory of Measuring Theory and Precision Instrument and the School of Instrument Science and Optoelectronics Engineering, Hefei University of Technology, Hefei, Anhui 230009, China (e-mail: hjxia@hfut.edu.cn).

Digital Object Identifier 10.1109/TIM.2025.3643072

In dynamic systems, directly measuring output variable y typically fails to capture the full range of uncertainty sources involved in the measurement process [6]. A common strategy is indirect evaluation [7]: one establishes a mapping $y = f(x)$ between the input variables x and the measurand y and then evaluates how uncertainty propagates through f . Depending on the method used to determine f , these methods can be categorized into analytical modeling and data-driven (experimental) modeling [6], [8]. The former creates a model based on the physical laws of the system that gives the relationship between the input and output quantities [3], [9]. However, due to the linear limitation of the uncertainty transfer model, analytical modeling has limitations in the uncertainty evaluation of nonlinear dynamic systems. Data-driven modeling, such as Monte Carlo method (MCM) [10] and gray system theory (GST) [11], estimate f through statistical analysis and curve fitting of the inputs and outputs of the system. However, MCM fundamentally relies on precise knowledge of the probability distribution of measurement data, while GST is critically sensitive to the representativeness of initial datasets and the repeated sampling of the initial sample data will increase additional uncertainty. Regardless of whether f is obtained analytically or learned from data, the resulting uncertainty is evaluated within the metrological framework for measurement systems [6]. However, to avoid ambiguity and potential confusion with the GUM-defined notion of measurement uncertainty, in the remainder of this article, we use the term “uncertainty” rather than “measurement uncertainty.”

Deep learning (DL), as a representative data-driven approach [12], [13], has exhibited outstanding capabilities in uncertainty quantification (UQ) for complex systems. This is largely attributed to its powerful nonlinear mapping ability and the rapid development of diverse uncertainty estimation techniques in recent years [14], [15]. These advancements have facilitated the successful application of UQ methods in various domains, including industrial process monitoring [16], biomedical signal processing [17], and meteorological forecasting [18], among others. However, purely data-driven DL models often lack generalizability and physical interpretability when applied to the modeling of complex dynamic systems, which in turn contributes to increased uncertainty in predictions. Physics-informed neural networks (PINNs), by integrating physical constraints with observational data, significantly enhance the model’s generalization ability and physical consistency [19]. However, when the system’s differential

equations contain unknown variables [20], the application of PINNs encounters significant challenges.

Common UQ methods in DL include Bayesian neural networks (BNNs) and ensemble methods (EMs), among others [14]. BNNs estimate the predictive distribution by incorporating Bayesian inference into DL models, while EMs leverage the averaging effect of multiple independently trained models to capture uncertainty. Despite their effectiveness, both approaches are computationally intensive and often suffer from low efficiency. In our previous studies [15], [16], we proposed a recurrent neural network (RNN)-based approach for modeling nonlinear dynamic systems and explored the use of EMs and evidential learning [21] for predictive uncertainty estimation. However, such purely data-driven methods lack physical interpretability in UQ, and the former also incurs high computational costs.

To model nonlinear dynamic systems and evaluate the uncertainty in their predictive outputs, this study proposes a DL framework, termed the physics-informed evidential network (PIENet). In this framework, the system's differential equations are incorporated as physical priors. By incorporating evidential learning, uncertainty-aware constraints are introduced during training, thereby enhancing the robustness of physical modeling and enabling the model to capture uncertainty in a single forward pass, significantly improving inference efficiency compared with BNNs and EMs. When the system's governing equations contain unknown variables, we use maximum likelihood estimation (MLE) to approximate their distributions, enabling the network to incorporate their effects into the uncertainty modeling process. This strategy compensates for incomplete physical knowledge and contributes to improved prediction reliability. We validate the proposed framework on general high-order nonlinear dynamic system datasets, including the publicly available Silverbox benchmark dataset and real-world experimental data obtained from a piezoelectric inertial drive system. It should be emphasized that the proposed PIENet provides a data-driven indirect uncertainty evaluation method within the context of dynamic measurements. Specifically, the uncertainty estimated by PIENet reflects the propagation and transformation of measurement-related uncertainties (sensor noise, environmental disturbances, and model imperfections) through the dynamic system model [6], [23]. Therefore, this work contributes to the uncertainty evaluation field by offering a computational complement to traditional evaluation methods, particularly for nonlinear dynamic systems where analytical uncertainty propagation is infeasible.

Compared with the existing literature on uncertainty evaluation in dynamic systems, our study has several unique advantages.

- 1) This study proposes a novel framework, which integrates PINNs with evidential learning to achieve uncertainty evaluation in dynamic systems while improving modeling efficiency.

- 2) By introducing an enhanced uncertainty-aware constraint mechanism, the model demonstrates improved physical consistency in the presence of unknown variables.

- 3) The proposed method has been effectively validated on both public and experimental datasets, demonstrating strong generalization capability and establishing a solid foundation for the engineering application of modeling and uncertainty evaluation in nonlinear dynamic systems.

II. RELATED WORK

A. Modeling Dynamic Systems With Purely Data-Driven DL Models

In recent years, DL has demonstrated remarkable performance and broad application potential in modeling complex dynamic systems [14]. Multilayer perceptron and radial basis function networks have obtained satisfactory results in simple dynamic system modeling (e.g., weather data prediction [18]). For more complex temporal dependencies, RNN architectures [15], [22] and their gated variants form deterministic models for modeling temporal data. Transformer architectures have made significant advances in modeling chaotic dynamic systems [24]. Dynamic variational autoencoders, as an extension of conventional variational autoencoders, have improved the ability to capture the latent state evolution of dynamic systems [25].

Despite the considerable progress achieved by the aforementioned methods in modeling dynamic systems, their physical interpretability remains limited due to the inherently “black-box” nature of neural networks.

B. Modeling Dynamic Systems With PINNs

PINNs establish a novel hybrid modeling paradigm by synergistically integrating data-driven modeling with analytical modeling [19]. The framework leverages two synergistic mechanisms: 1) utilizing neural networks as universal approximators to encode high-dimensional representations of system responses and 2) embedding physics-informed constraints (e.g., differential equation and initial or boundary conditions) to formulate multiobjective optimization problems. This dual-driven approach improves generalization under sparse data by enforcing physical constraints and enhancing interpretability. Recent studies have demonstrated the remarkable capability of PINNs in modeling complex nonlinear systems, including successful reconstruction of pressure, temperature, and velocity fields in nanofluid convection, highlighting their effectiveness in thermal-fluid modeling [26]. Additionally, PINNs have been utilized for response estimation and parameter identification in structural dynamics systems, providing accurate state estimations even with sparse sensor data [27]. In robotics, PINNs have been employed for accurate state estimation and dynamic prediction [28]. However, there are challenges in the application of PINNs when the coefficients of the differential equations are not fully known [20]. Moreover, the original PINNs framework lacks a systematic mechanism for UQ, making it difficult to reliably assess the confidence of the predictions.

Compared to traditional PINNs, the proposed approach combines uncertainty-aware loss with physics-based loss, leading to improved model robustness when dealing with complex systems.

C. Uncertainty in Neural Network Models

Measurement uncertainty refers to the dispersion reasonably attributable to an estimated measurand value derived from observed measurement data using mathematical estimation methods. In practical measurements, the uncertainty of a measurement result is influenced by multiple factors, including measurement noise, repeatability, calibration errors,

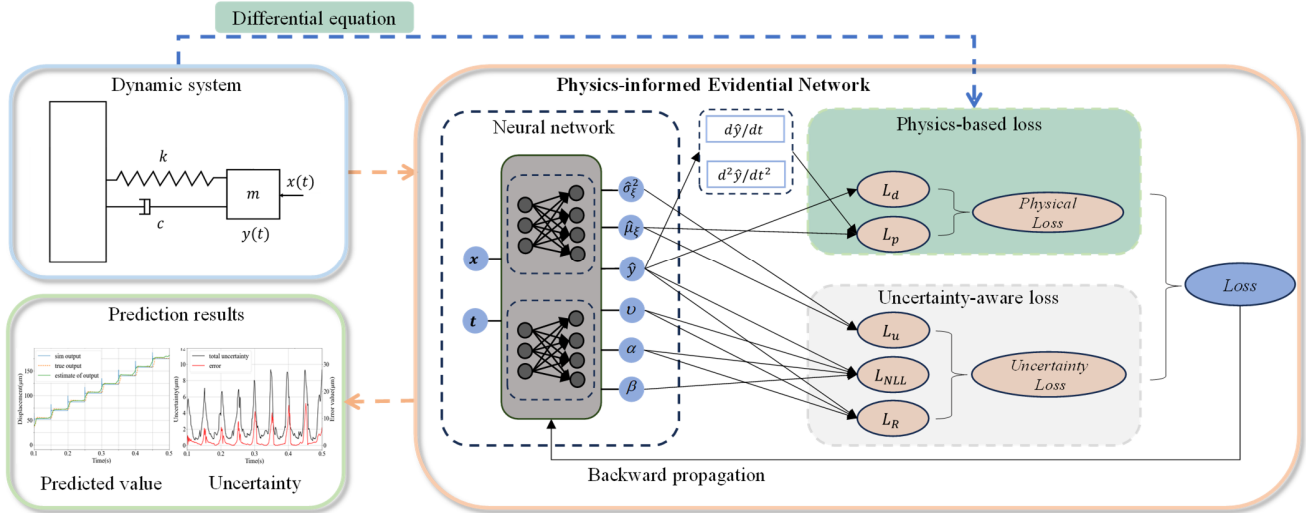


Fig. 1. Process of the proposed method for dynamic system modeling and uncertainty evaluation.

environmental conditions, and model parameter uncertainties. All these factors jointly determine the uncertainty of the estimated measurement value and influence the measurement result.

In the proposed framework, the observed data is used as training for the model. Model uncertainty estimated by network models represents epistemic effects such as limited data, model parameter errors, and unmodeled dynamics [30]. In contrast, data uncertainty corresponds to stochastic measurement-related noise contained in the data itself, typically caused by sensor limitations, environmental fluctuations, or labeling errors. Together, these two components encompass the main factors affecting the reliability of measurement results. In practice, the total uncertainty can be interpreted as the superimposed effect of model uncertainty and data uncertainty [16]. Our study focuses on this total uncertainty, acknowledging that reliable uncertainty evaluation requires comprehensive consideration of all contributing factors affecting the measurement outcome.

Various methods have been developed to estimate predictive uncertainty in neural networks. BNNs approximate uncertainty using variational inference or stochastic sampling. They have demonstrated success in quantifying uncertainty consistent with prediction errors in 3-D shape reconstruction tasks [31] and have effectively enhanced diagnostic reliability in medical imaging applications [32]. EMs aggregate predictions from multiple independent models to capture composite uncertainty, and have demonstrated notable effectiveness in tasks such as optical system calibration [33] and industrial defect detection [34]. Compared with other uncertainty estimation methods such as BNN [35] and EMs [36], as a deterministic method for estimating uncertainty, evidential network (ENet) places priors on the likelihood function and outputs hyperparameters of high-order evidence distribution by training neural networks, providing higher computational efficiency and simpler model architecture [21].

To address the aforementioned limitations, this study proposes a hybrid modeling approach that integrates ENet with PINNs for the modeling and uncertainty evaluation of dynamic systems. Recent studies have also explored similar

combinations. For instance, E-PINN [37] replaces the original evidential regularizer with a combination of Kullback–Leibler (KL) divergence and error-weighted terms, while PINN-DERs [38] propose substituting the loss function of evidential regression with the residuals of partial differential equations (PDEs). Although these approaches demonstrate architectural innovations, they do not specifically target dynamic measurement problems and largely overlook the challenge of integrating PINNs with evidential frameworks when the governing differential equations are incomplete or contain unmodeled disturbances. This study aims to fill this gap by offering a systematic solution tailored to such scenarios.

III. METHODOLOGY

In this article, to evaluate the uncertainty of nonlinear dynamic systems, we propose a hybrid modeling evaluation framework, PIENet, which combines physical priors with evidential learning to accommodate situations, where the differential equations governing nonlinear dynamic systems contain missing or unknown components. The process of our proposed method is shown in Fig. 1. First, the output response and the input signal of the dynamic system are sampled synchronously by a multisensor array, followed by chronological partitioning into training sets and test sets with normalization. Second, construct a residual-enhanced dual-branch feedforward network, where the first branch estimates posterior parameters for unknown terms in governing equations, and the second branch predicts target distribution parameters. Third, a composite loss function incorporating both physical loss and uncertainty loss is constructed and jointly optimized. Fourth, feed the test dataset into the trained neural network to compute the predicted outputs and their associated uncertainty.

A. PIENet Framework

To address unquantifiable nonlinear dynamic disturbances $\xi(t)$ (e.g., unmodeled friction dynamics and time-varying hysteresis) in dynamic measurement systems, we formulate

the system as a differential equation with latent disturbances [39]

$$F\left(y, x, \xi, t, \frac{dy}{dt}, \frac{d^2y}{dt^2}, \dots\right) = 0, x \in A, t \in [0, T] \quad (1)$$

where F is a nonlinear function, A is a subset of \mathbb{R}^D , and the output variable $y(t_i)$ is a function of the time-dependent input signal $x(t_i)$ and time $t_i (i = 0, 1, \dots, N)$. We assume that $\xi(t_i)$ is a time-dependent stochastic process. At each time instance t_i , $\xi(t_i)$ is modeled as a normally distributed random variable with mean $\mu_{\xi(t_i)}$ and variance $\sigma_{\xi(t_i)}^2$

$$\xi(t_i) \sim N(\mu_{\xi(t_i)}, \sigma_{\xi(t_i)}^2). \quad (2)$$

In this work, the dataset comprises time-series input–output pairs collected from real-world dynamic systems. It includes both single-segment discrete signals sampled over time and multiple signal segments generated under different input conditions (e.g., varying frequency or amplitude). Such a setting allows our method to be flexibly applied to a wide range of nonlinear dynamic systems and excitation patterns.

The system dynamics function F is approximated by a fully connected neural network $F_{\text{NN}}(\theta)$, as followed in [19]. We take the time-varying signals $x(t_i)$ and temporal sequence t_i as network inputs and outputs the predicted value $\hat{y}(t_i; \theta)$ of the system response $y(t_i)$. The neural network consists of multiple hidden layers, with the input and output of each layer propagated through the network as follows:

$$h^{(l)} = f_{\text{act}}(w^{(l)} h^{(l-1)} + b^{(l)}), l = 1, 2, \dots, L \quad (3)$$

where $h^{(l)}$ denotes the output of the l th layer; $w^{(l)}$ and $b^{(l)}$ are the trainable weights and bias, respectively; $f_{\text{act}}(\cdot)$ is a nonlinear activation function; and L is the total number of layers. The neural network parameters are optimized by minimizing a composite loss function that integrates physics-based loss derived from system differential equations with an uncertainty-aware loss. The specific formulation of this loss function is detailed in Section III-B.

B. Loss Function

In this section, we propose a loss function that integrates physical information with uncertainty-aware learning. The physical information is enforced through the residuals of the system's differential equations, while the uncertainty constraint is achieved via a dual-objective optimization that combines the MLE of the unknown variables with the evidential learning loss of the predicted outputs.

1) *Physics-Based Loss*: We differentiate the predicted $\hat{y}(t_i; \theta)$ and substitute it into the differential equations, aiming to minimize the residuals of these equations to guide the neural network toward improved generalization and convergence to physically consistent solutions. However, due to the presence of unknown variables ξ in the differential equations, directly computing the residuals using (1) neglects the uncertainty of ξ , as well as its dynamic coupling with the system state. This may lead to an inability to accurately capture the true physical behavior of the system. To address this, we approximate ξ by its predicted mean $\hat{\mu}_{\xi(t_i; \theta)}$, which is learned from data. We

minimize the residuals of the differential equations to optimize the parameters θ of the network

$$L_p(\theta) = \frac{1}{N_p} \sum_{i=1}^{N_p} \left| F\left(\hat{y}, x, \hat{\mu}_{\xi}, t_i, \frac{d\hat{y}}{dt_i}, \frac{d^2\hat{y}}{dt_i^2}, \dots\right) \right|^2 \quad (4)$$

where N_p represents the number of physics-informed collocation points. In the following section, we provide a detailed explanation of the origin of $\hat{\mu}_{\xi(t_i; \theta)}$.

In addition, we incorporate a mean squared error (MSE) loss to improve the accuracy of the model's point estimates

$$L_d(\theta) = \frac{1}{N_d} \sum_{j=1}^{N_d} |\hat{y}(t_j; \theta) - y(t_j)|^2 \quad (5)$$

where N_d represents the number of samples of training data. L_d intends to minimize the discrepancy between \hat{y} and y , thereby enhancing model accuracy. Thus, the physics-based loss L_{Phy} of PIENet is defined as

$$L_{\text{Phy}} = L_p + L_d. \quad (6)$$

2) *Uncertainty-Aware Loss*: When latent disturbances become nonnegligible, they can be regarded as missing variables in the system's governing differential equations. Under such circumstances, accurately modeling the underlying dynamics and systematically assessing predictive uncertainty become highly challenging. We construct a hierarchical probabilistic modeling framework with dual optimization objectives: 1) to enhance model robustness against dynamical disturbances by minimizing the negative log-likelihood loss of missing variables ξ and 2) to achieve a unified representation of model and data uncertainty by jointly optimizing higher order distribution parameters and predictive variance within the evidential regression framework.

We propose to constrain the variation domain of missing variables through statistical distribution modeling. Specifically, a neural network predicts distribution parameters [assuming a normal distribution, see (2)] for unknown dynamic variables through nonlinear mappings. Following the MLE principle, maximizing the likelihood of ξ is reformulated as minimizing the negative log-likelihood loss:

$$L_u(\theta) = \frac{1}{N_p} \sum_{i=1}^{N_p} \frac{(\xi(t_i) - \hat{\mu}_{\xi(t_i; \theta)})^2}{\hat{\sigma}_{\xi(t_i; \theta)}^2} + \log \hat{\sigma}_{\xi(t_i; \theta)}^2 \quad (7)$$

where $\hat{\sigma}_{\xi(t_i; \theta)}^2$ represents the predicted variance of $\xi(t_i)$ at time t_i , produced by the network. Here, the reference value of $\xi(t_i)$ is used in place of the inaccessible ground truth, under the assumption that it shares the same underlying distribution. The derivative of the measurement sequence is estimated using the fourth-order central difference method, followed by physical inversion based on the governing differential equation to obtain the reference value of $\xi(t_i)$.

Consider that the system output variable $y(t_i)$ at a particular point t_i (hereafter, subscript i denotes the time step t_i and $\hat{y}(t_i; \theta)$ is simplified to \hat{y}_i) is sampled from an unknown Gaussian distribution $y_i \sim N(\mu_i, \sigma_i^2)$, serving as the conjugate prior for the normal distribution, where the unknown μ_i follows a normal distribution, and the unknown σ_i^2 follows an inverse-gamma distribution [21]:

$$y_i | \mu_i, \sigma_i^2 \sim N(y_i | \mu_i, \sigma_i^2) \quad (8)$$

$$\mu_i, \sigma_i^2 | \hat{y}_i, v_i, \alpha_i, \beta_i \sim N(\mu_i | \hat{y}_i, \sigma_i^2 / v_i) \Gamma^{-1}(\sigma_i^2 | \alpha_i, \beta_i) \quad (9)$$

where α_i and β_i denote the shape and scale parameters of the gamma distribution, respectively, and v_i represents the number of virtual observations used in estimating the mean of the target variable and characterizes the strength of confidence in the prior knowledge. $\Gamma(\cdot)$ denotes the gamma distribution. Let $\phi_i = (\mu_i, \sigma_i^2)$ denote the model parameter, to estimate the posterior distribution $p(\phi_i | y_i)$ of ϕ_i and ensure that the predictive distribution of y_i closely approximates the true distribution, a normal inverse-gamma (NIG) distribution $p(\phi_i | I_i)$ is used to approximate the posterior, where $I_i = \{\hat{y}_i, v_i, \alpha_i, \beta_i\}$ denotes the NIG distribution parameter. By marginalizing over parameter μ_i and σ_i , the conditional probability distribution of y_i is

$$\begin{aligned} p(y_i | I_i) &= \int_{\sigma_i^2=0}^{\infty} \int_{\mu_i=-\infty}^{\infty} p(y_i | \mu_i, \sigma_i^2) p(\mu_i, \sigma_i^2 | \hat{y}_i, v_i, \alpha_i, \beta_i) d\mu_i d\sigma_i^2 \\ &= St\left(y_i; \hat{y}_i, \frac{\beta_i(1+v_i)}{v_i\alpha_i}, 2\alpha_i\right) \end{aligned} \quad (10)$$

where $St(\cdot)$ denotes the t -distribution. The network parameters θ are optimized by minimizing the negative log marginal likelihood (NLL) function, effectively maximizing the model evidence to achieve a better fit to the observed data

$$\begin{aligned} L_{\text{NLL}}(\theta) &= \frac{1}{N_d} \sum_{i=1}^{N_d} \frac{1}{2} \log\left(\frac{\pi}{v_i}\right) - \alpha_i \log(\Omega_i) \\ &\quad + \left(\alpha_i + \frac{1}{2}\right) \log((y_i - \hat{y}_i)^2 v_i + \Omega_i) \\ &\quad + \log\left(\frac{\Gamma(\alpha_i)}{\Gamma(\alpha_i + \frac{1}{2})}\right) \end{aligned} \quad (11)$$

where $\Omega_i = 2\beta_i(1 + v_i)$. To avoid the risk of misleading evidence caused by the model being overly confident in incorrect predictions, we introduce a regularization term in the loss function to constrain the model's confidence in its outputs

$$L_R(\theta) = \frac{1}{N_d} \sum_{i=1}^{N_d} |y_i - \hat{y}_i| (2v_i + \alpha_i). \quad (12)$$

The final expression of the uncertainty-aware loss L_{Unc} is

$$L_{\text{Unc}} = \lambda_u L_u + L_{\text{NLL}} + \lambda_R L_R \quad (13)$$

where $\lambda_u (0 < \lambda_u < 1)$ is a weighting factor used to balance the relative importance between the uncertainty of the unknown variables and the predictive uncertainty of the model output, and λ_R represents the regularization parameter, which is typically set to a default value of 0.01 [21].

Then, we derive the loss function of our proposed PIENet, denoted as

$$L = L_{\text{Phy}} + L_{\text{Unc}}. \quad (14)$$

The total predictive uncertainty U_{total} is obtained by combining the data uncertainty U_{data} and model uncertainty U_{model} under the assumption that they are statistically independent. In this case, the total uncertainty is computed based on the variance additivity rule [4], [31] as

$$U_{\text{total}} = \sqrt{U_{\text{data}}^2 + U_{\text{model}}^2} \quad (15)$$

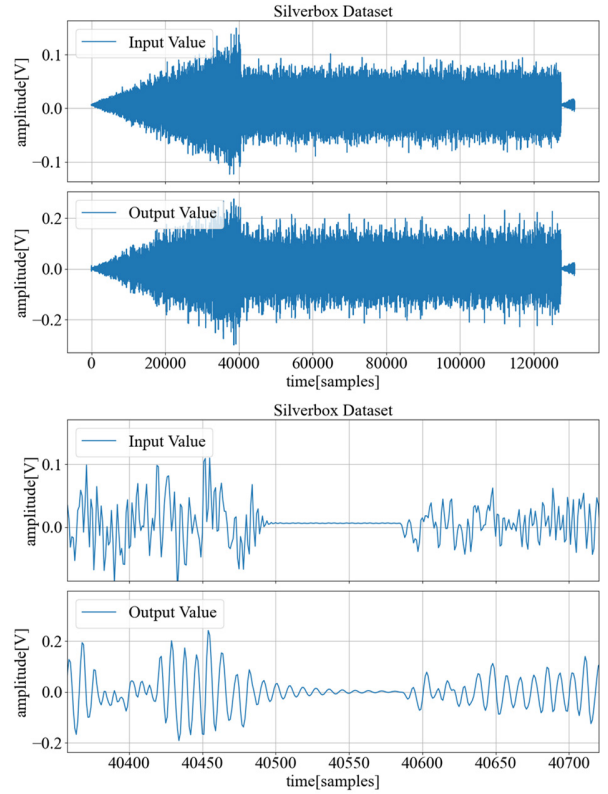


Fig. 2. Dataset of the Silverbox. Input–output data from the Silverbox (top) and detailed view of samples at the boundary (bottom).

where in the evidential regression

$$U_{\text{data}} = \sqrt{\int_{\sigma^2=0}^{\infty} \sigma^2 p(\sigma^2) d\sigma^2} = \sqrt{\frac{\beta}{\alpha-1}} \quad (16)$$

$$U_{\text{model}} = \sqrt{\int_{\mu=-\infty}^{\infty} \mu^2 p(\mu) d\mu - (E[\mu])^2} = \sqrt{\frac{\beta}{v(\alpha-1)}} \quad (17)$$

where α and β control the shape and scale of the predicted distribution, determining the magnitude and convergence characteristics of the predictive variance. The parameter v reflects the confidence in prior knowledge; a larger v leads to a more stable predicted mean and lower uncertainty. Together, these parameters shape the evidential distribution, enabling the explicit decomposition of data and model uncertainty.

IV. EXPERIMENTS

In this section, we evaluate the performance of the proposed modeling approach, PIENet, in reconstructing physically meaningful network models and evaluating uncertainty from experimental data of nonlinear dynamic systems. Here, uncertainty refers to the overall dispersion parameter associated with the estimated measurand, arising from combined sources of uncertainty in system operation, sensor measurements, and neural network modeling and inference. The following models are employed as experimental cases in this study: 1) the Silverbox dataset utilizing real-world experimental data [40] and 2) experimental measurement data from piezoelectric

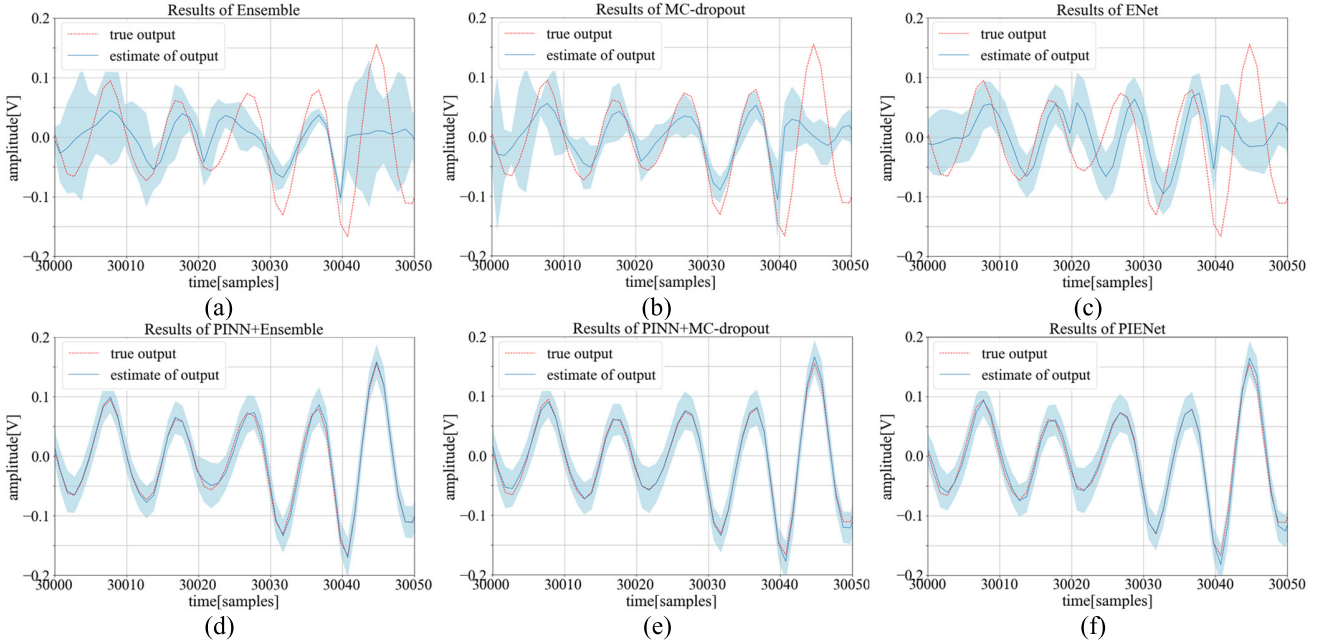


Fig. 3. Test results of different approaches on the test set. (a) EM and (d) fusion of PINN and EM. (b) MC-dropout method and the fusion of PINN and (e) MC-dropout method. (c) ENet and (f) our proposed method. The shaded area indicates the uncertainty.

inertial drive systems [41]. In the first case study, we focus on evaluating the generalization performance of PIENet in modeling nonlinear dynamic systems and demonstrate its effectiveness and efficiency in identifying and capturing the true underlying uncertainty within such systems. The second case focuses on the ability of PIENet to learn the underlying mathematical model of a measurement system from real-world observational data in the presence of missing variables in the system model. This demonstrates the modeling capacity and uncertainty estimation effectiveness of our method under this specific and challenging scenario.

We emphasize that our method is not intended as a substitute for existing dynamic system modeling techniques, but rather serves as a demonstration of the efficacy of neural network methods in nonlinear dynamic system modeling and uncertainty evaluation.

A. Silverbox System Benchmark

1) *System Description:* The Silverbox system, designed to simulate the nonlinear mechanical oscillation process, can be approximately described by the following second-order differential equation:

$$m \frac{d^2y(t)}{dt^2} + c \frac{dy(t)}{dt} + ky(t) + k_n y^3(t) = x(t) \quad (18)$$

where $x(t)$ represents the time-varying signal input and $y(t)$ denotes the displacement of the mass block, $m = 9.83 \times 10^{-6}$, both represented by voltage values. $k = 15.1 \times 10^4$ and $k_n = 40.62 \times 10^4$ represent the elastic coefficients of the nonlinear asymptotic spring, and $c = 25.32$ represents the viscous damping coefficient [42]. This constitutes a nonlinear dynamic system characterized by a single input and a single output, wherein data noise is intrinsic to the measurements. As shown in Fig. 2(a), the dataset comprised two components. The first part consisted of 40 000 samples of Gaussian white

TABLE I
PERFORMANCE OF DIFFERENT METHODS IN SILVERBOX SYSTEM BENCHMARK

Metrics Methods	RMSE	Inference Speed (s)
PINN + Ensemble	0.0389	0.12
PINN + MC-dropout	0.0384	0.11
PIENet	0.0388	0.04

noise ranging linearly in amplitude from zero to its maximum value over the interval from $t = 1$ to $t = 40\ 000$, which served as the test set. The second part consisted of 91 072 samples, representing ten randomly odd multiplicative sine functions continuously combined over the interval $t = 40\ 001$ to $t = 131\ 072$, forming the original training set. In this study, the Gaussian white noise samples persisted until $t = 40\ 585$, as shown in Fig. 2(b). To demonstrate the modeling and generalization capabilities of PIENet, we used 40 000 samples from $t = 40\ 586$ to $t = 80\ 586$ as the training set, following the setup described in [40].

2) *Results:* Based on the Bayesian optimization method [43], we adopted a fully connected neural network architecture consisting of four hidden layers, each containing 128 neurons. The model was trained using the Adam optimizer with a learning rate of 1×10^{-4} in this case.

Fig. 3 illustrates the performance of different methods on the test set, with a selected local analysis window ranging from $t = 30\ 000$ to $t = 30\ 050$ for a more detailed comparison. We evaluate the proposed method by comparing its fitting performance and inference speed with (a) EMs (with an ensemble size of 8), (c) MC-dropout (interpreted as a variational approximation to BNN) [14], and (e) ENet and hybrid approaches that combine PINN with the first two uncertainty estimation techniques. The comparative results of the three PINN-based models are

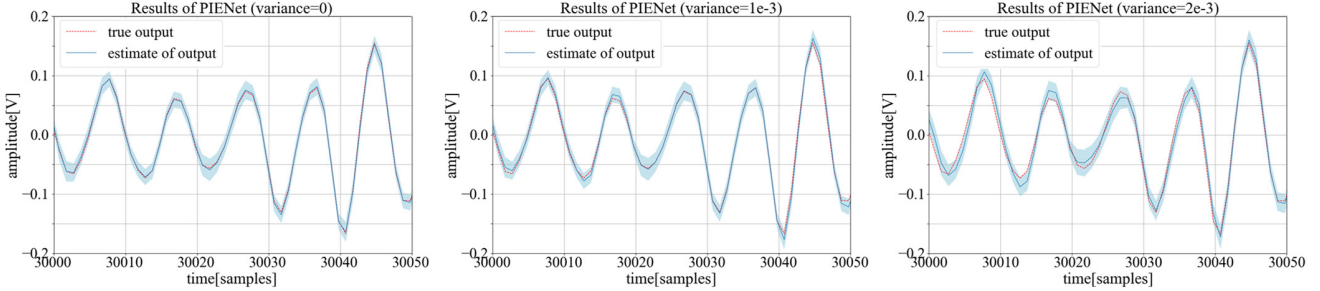


Fig. 4. PIENet test results with different levels of zero-mean Gaussian noise. No noise(left). Gaussian noise with variance $1e^{-3}$ (middle). Gaussian noise with variance $2e^{-3}$ (right).

TABLE II
ERROR AND UNCERTAINTY UNDER DIFFERENT NOISES

Noise level	Mean of the error	Mean of the uncertainty	Correlation coefficient
0	1.5e-3	8e-3	0.78
1e-3	2.0e-3	1.7e-2	0.75
2e-3	4.8e-3	2.5e-2	0.67

presented in Table I, where we report the root mse (RMSE) of the predictions and the corresponding inference times. To ensure fairness and comparability, all models are trained and tested on the same dataset. It is important to emphasize that the objective of this study is to compare our method with general-purpose methods under typical conditions, rather than to identify optimal hyperparameters of all methods.

As shown in Fig. 3, the integration with PINN enhances the model's generalization capability. Compared to the first two hybrid methods, the proposed approach demonstrates competitive performance in both fitting accuracy and inference speed. This is because PINN + Ensemble relies on aggregating outputs from multiple independently trained models, and PINN + MC-dropout requires multiple forward passes for sampling. In contrast, PIENet achieves efficient inference through a single forward pass while still capturing consistent predictive uncertainty. These results validate the effectiveness of PIENet in modeling nonlinear dynamic systems and quantifying associated uncertainty.

To further investigate the capability of the proposed method in capturing uncertainty, we introduce additive Gaussian white noise with zero mean and varying variances to the test signals, simulating measurement noise during the data acquisition process. The results shown in Fig. 4 indicate that, under the same confidence level ($P = 95\%$), the noise intensity affects the model's test outcomes, causing deviations in the predictions and leading to changes in uncertainty. As shown in Fig. 4, a clear correlation is observed between the prediction error and the estimated uncertainty within the temporal window. Data points with higher predictive uncertainty tend to exhibit larger prediction errors [45]. We compared the mean prediction error and the mean estimated uncertainty within each temporal window and computed their correlation, as shown in Table II. The experimental results demonstrate a strong correlation between the two. This sensitivity to input noise and the observed association with prediction bias indicate that the

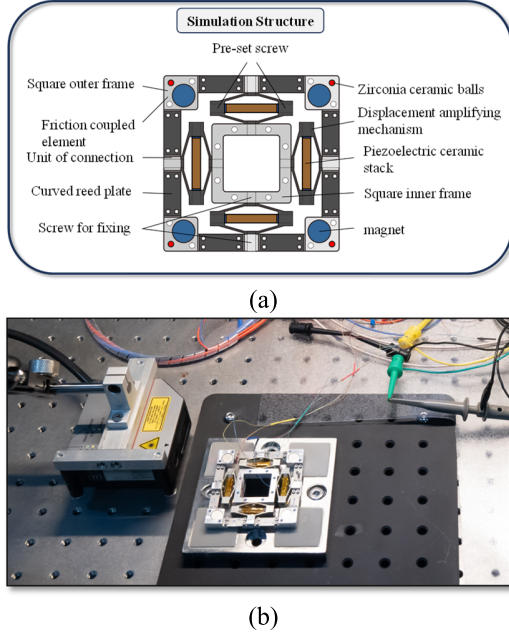


Fig. 5. Piezoelectric inertial driving experimental device. (a) Structure of the simulation model. (b) Laser displacement sensor measures displacement in piezoelectric inertial drive system.

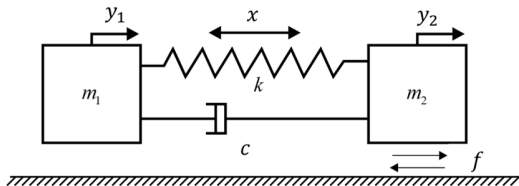


Fig. 6. Dynamic modeling of piezoelectric inertial driving experimental device.

uncertainties estimated by PIENet reasonably reflect noise-induced prediction deviations. Although the ground truth of uncertainty is not directly accessible, the proposed method provides a valuable foundation for risk assessment in practical engineering applications.

B. Piezoelectric Inertial Drive System

1) *System Description:* The operational principle of piezoelectric ceramic actuators is based on the inverse piezoelectric effect of piezoelectric ceramics [41]. The experimental setup of

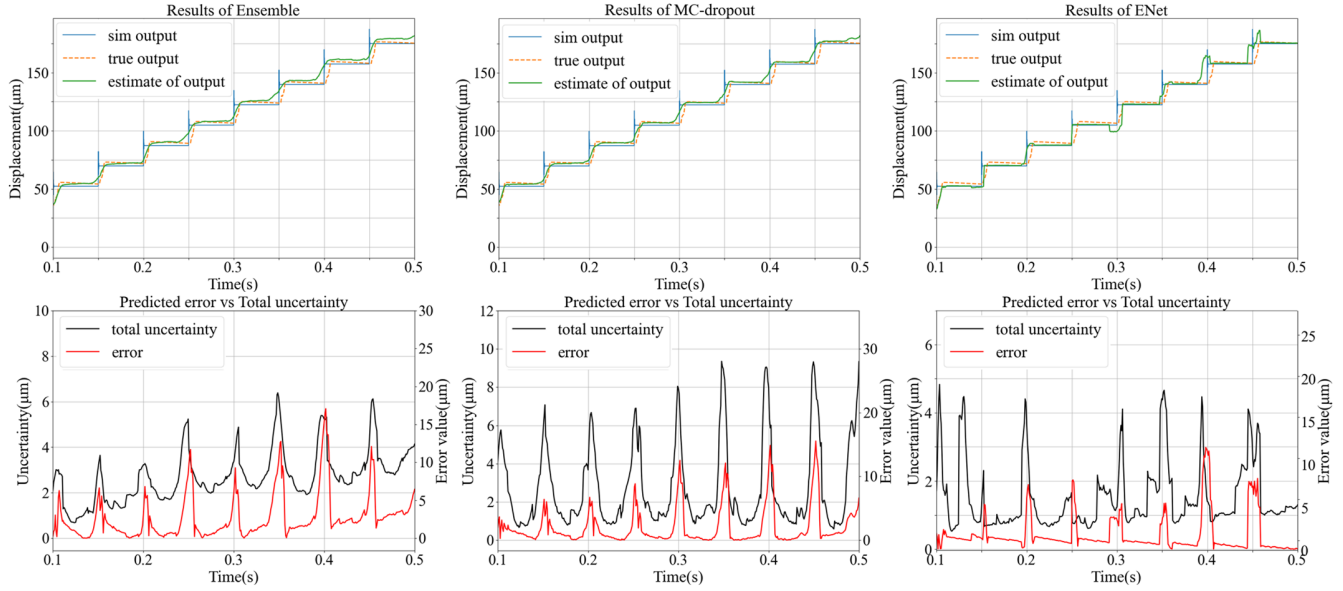


Fig. 7. Performance comparison of different uncertainty modeling methods: EM (left), MC-dropout (middle), and ENet (right).

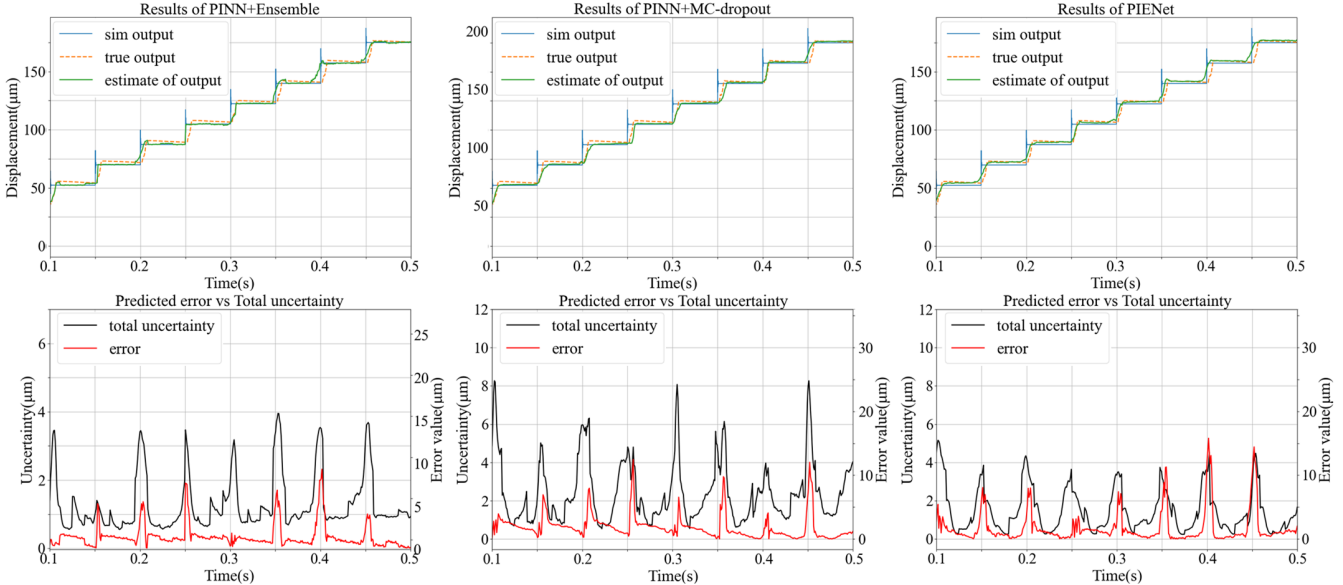


Fig. 8. Performance comparison of different methods after integration with PINNs. Simple fusion of PINN and EM (left), simple fusion of PINN and MC-dropout method (middle), and our proposed method (right).

the piezoelectric inertial driving device is shown in Fig. 5. Its operational principle exploits the rapid deformation generated by the piezoelectric elements upon rapid electrical excitation, thereby generating a powerful inertial impact force. This force, in turn, impels the mover to overcome the frictional forces between the contact surfaces, resulting in minute displacement. Typically, a continuous sequence of inertial impact is induced by a periodic sawtooth wave signal that facilitates the continuous motion of the mover. The magnitude of the inertial impact force is modulated by adjusting the duty cycle and amplitude of the sawtooth wave signal.

In accordance with the structural characteristics of piezoelectric inertial driving systems, they are commonly simplified into spring–mass–damping systems, as depicted in Fig. 6. The inertial body m_1 undergoes displacement y_1 under the

influence x of the driving force exerted by the piezoelectric ceramic. The actuator m_2 experiences displacement y_2 due to the inertial impact force. Considering the nonlinear frictional force f acting on the mover, the dynamic equations can be expressed as

$$\begin{cases} m_1 \frac{d^2 y_1}{dt^2} = -x + k(y_2 - y_1) + c \left(\frac{dy_2}{dt} - \frac{dy_1}{dt} \right) \\ m_2 \frac{d^2 y_2}{dt^2} = x - k(y_2 - y_1) - c \left(\frac{dy_2}{dt} - \frac{dy_1}{dt} \right) - f. \end{cases} \quad (19)$$

Let $y = y_2 - y_1$ represent the overall displacement of the drive platform, $c = 83$ denote the damping coefficient, and $k = 10.27 \times 10^6$ denote the stiffness of the equivalent spring.

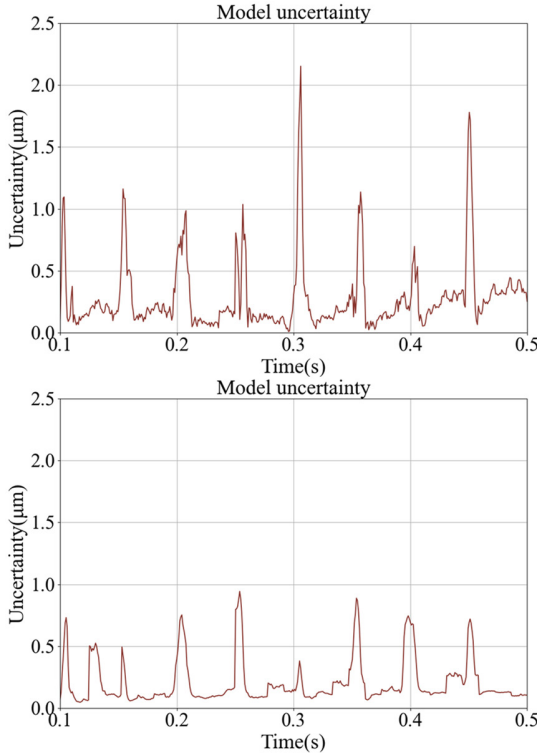


Fig. 9. Comparison of model uncertainty of test results for ENet (top) and our proposed method (bottom).

We can rewrite (19) as

$$\begin{aligned} \frac{d^2y}{dt^2} + c \frac{m_1 + m_2}{m_1 m_2} \frac{dy}{dt} + k \frac{m_1 + m_2}{m_1 m_2} y + \frac{f}{m_2} \\ = \frac{m_1 + m_2}{m_1 m_2} x \end{aligned} \quad (20)$$

where $m_1 = 0.132$, $m_2 = 0.0116$, and $x = \delta V$ is determined by the input voltage V of the piezoelectric ceramic, in which $\delta = 2.4$.

To investigate the generalization capability of PIENet in dynamic system modeling, we used a laser displacement sensor to measure the continuous driving displacement of a piezoelectric ceramic driving system over ten cycles and constructed an experimental dataset. This dataset includes input-output data of the driving system under 11 different frequencies, driven by input voltage signals with varying amplitudes. For each frequency, the input comprises 40 sawtooth wave voltage signals with peak-to-peak amplitudes ranging from 30 to 120 V, and a duty cycle of 0.9999. Under each peak-to-peak voltage, ten cycles of input voltage signals and their corresponding displacement outputs were collected as a mapping pair. The frequency range spans from 5 to 40 Hz, resulting in a total of 11×40 mapping pairs in the dataset.

During actual system operation, external noise, measurement limitations, and temperature fluctuations introduce significant unpredictability in the behavior of f . Therefore, we treat f as missing variables ξ and employ two independent feedforward neural networks to output the estimated mean and variance of f , and the parameters of evidential distribution. In this case, we selected a neural network architecture with five hidden layers, each comprising 200 neurons. The model

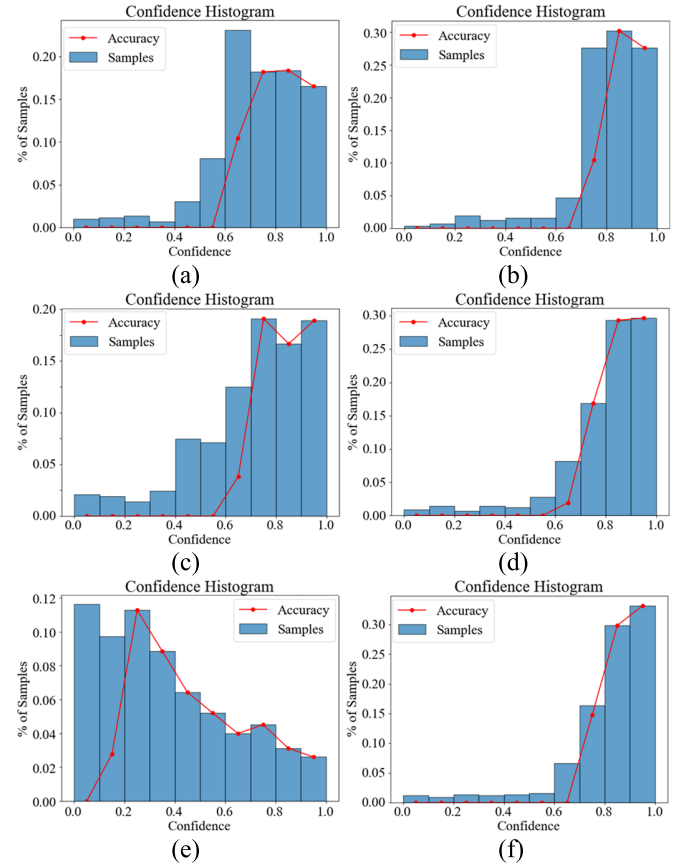


Fig. 10. Confidence calibration results based on the predictions of different methods are visualized. (a) EM. (b) Simple fusion of PINN and EM. (c) MC-dropout method. (d) Simple fusion of PINN and MC-dropout method. (e) ENet. (f) Our proposed method.

was trained using the Adam optimizer with a learning rate of 1×10^{-4} .

To validate the learning capability and uncertainty evaluation performance of the proposed method on the experimental dataset, we compared it ($\lambda_u = 0.6$) with the aforementioned methods on the test set. Fig. 7 presents the performance comparison of different uncertainty modeling methods on the test dataset with an input voltage of $V = 80$ V, including the EM, the MC-dropout method, and the ENet method. Fig. 8 further illustrates the results of combining the first two methods with a basic PINN framework, as well as the performance of the proposed approach. In this comparison, the integration of Ensemble and MC-dropout with PINN was implemented by neglecting the influence of f . It is worth noting that all these methods are implemented using fully connected neural networks.

2) *Results:* As shown in Figs. 7 and 8, compared to our proposed method, other approaches exhibit certain limitations in capturing the true displacement behavior. The uncertainty curves display periodic fluctuations approximately every 0.05 s, which closely align with the trend of prediction errors. This consistency indicates that the uncertainty estimates produced by our model are reasonably reliable [45]. This phenomenon can be attributed to the operating frequency of the piezoelectric actuator, which is 20 Hz. A periodic sawtooth waveform is applied every 0.05 s, inducing dynamic responses in the

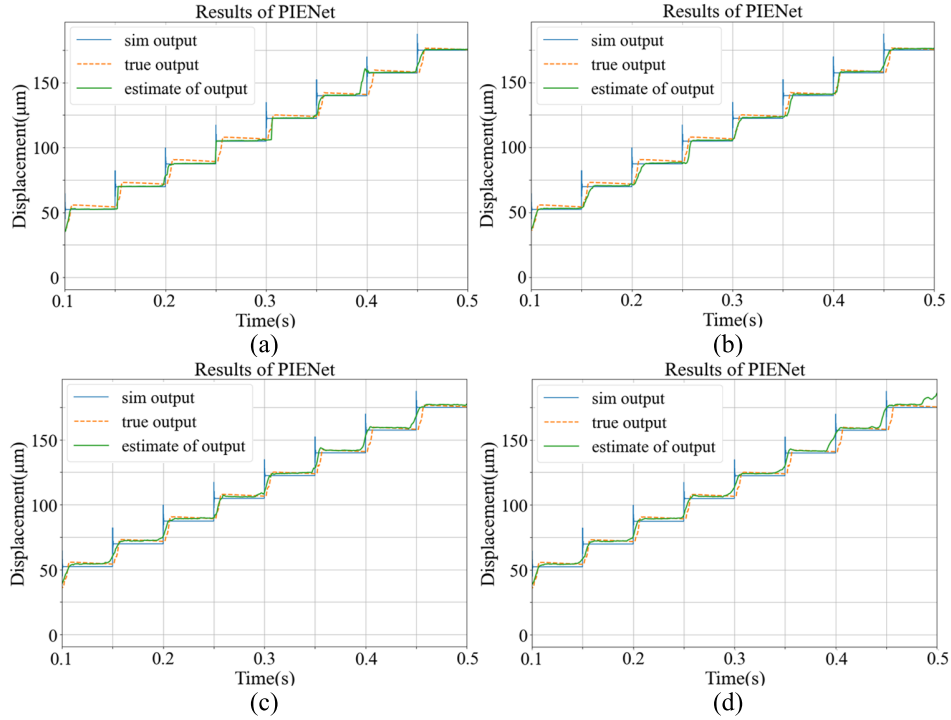


Fig. 11. Performance of our proposed method on the test set with different weights λ_u . (a) $\lambda_u = 0.01$. (b) $\lambda_u = 0.2$. (c) $\lambda_u = 0.6$. (d) $\lambda_u = 0.99$.

TABLE III

PERFORMANCE OF DIFFERENT METHODS IN PIEZOELECTRIC INERTIAL DRIVE SYSTEM

Metrics Methods \ Metrics	RMSE	R^2	Correlation coefficient
Ensemble	3.9082	0.997065	0.564
PINN + Ensemble	3.1028	0.997625	0.506
MC-dropout	3.6486	0.997414	0.583
PINN + MC-dropout	2.9866	0.997931	0.513
ENet	5.2130	0.994738	0.335
PIENet	2.9031	0.998336	0.758

actuator's internal circuitry. These responses are subject to time-varying and stochastic characteristics due to factors such as material degradation, mechanical fatigue, and external vibrations. Consequently, significant uncertainty arises at the moments of displacement transitions.

Fig. 9 compares the predicted model uncertainty between the baseline ENet method and our proposed method on the test dataset. It is clearly observed that our method substantially reduces the model uncertainty, demonstrating that incorporating physical information contributes to improved reliability of the model predictions.

Table III presents a quantitative comparison of the prediction accuracy of different methods on the test dataset, using RMSE and coefficient of determination (R^2) as evaluation metrics. In addition, it reports the correlation coefficients between prediction error and predicted uncertainty for each method, providing insight into the reliability of their uncertainty estimation. These indicators are calculated based on the observed

system outputs y as ground truth. The results demonstrate that the PIENet model outperforms other approaches in terms of prediction accuracy, indicating superior fitting capability and generalization performance. Moreover, the higher correlation coefficient between prediction error and predicted uncertainty suggests that the uncertainty estimates produced by PIENet are more reliable and better calibrated [46]. To further validate the accuracy of uncertainty evaluation for the different methods [44], we employ confidence–coverage plots to visualize the reliability of the predicted uncertainties, as shown in Fig. 10, which illustrates the calibration results under different confidence levels. Compared with methods without the incorporation of physical constraints [Fig. 10(a), (c), and (e)], the approaches integrating PINNs [Fig. 10(b), (d), and (f)] exhibit a substantial improvement in calibration behavior. Although the visual difference between our method [Fig. 10(f)] and certain competitive PINN-based approaches [e.g., Fig. 10(b) and (d)] appears less pronounced, our results consistently follow the theoretically desirable trend: the proportion of ground-truth samples captured within the prediction intervals increases steadily with higher confidence levels. This behavior reflects a well-calibrated uncertainty estimation and further confirms the reliability of the proposed PIENet in quantifying predictive uncertainty.

Next, we consider the impact of using different weighting coefficients λ_u on the test results. The parameter λ_u is used to balance the contribution of the uncertainty associated with the predicted output \hat{y} and that of the unknown variables. As illustrated in Fig. 11, a small value of λ_u may cause the model to underemphasize the influence of unknown variables in the differential equation, making it difficult to capture the complex dynamics present in real-world measurement systems. In particular, the model may struggle to effectively

infer the latent physical mechanism of nonlinear friction forces during the measurement process from limited observational data. As a result, the predictions tend to align more closely with the idealized simulation model (i.e., the solution of the physical differential equation), deviating from the true system outputs. Conversely, an excessively large λ_u may impair the model's ability to learn the true behavior of the predicted output \hat{y} , thus reducing its overall modeling accuracy. This variation in performance with respect to λ_u highlights the importance of balancing uncertainty constraints and physical consistency for ensuring model robustness.

V. CONCLUSION AND OUTLOOK

To evaluate the uncertainty of nonlinear dynamic systems, this article proposes a PIENet for indirect uncertainty evaluation. This method integrates physical constraints with uncertainty-aware constraints, enabling the learning of fundamental relationships in complex systems while reliably estimating the uncertainty in predictions. The proposed method is systematically validated on both public datasets and experimental datasets, and the results demonstrate that PIENet has excellent performance in terms of model fitting accuracy and computational efficiency. Moreover, recognizing that the true value is typically unavailable in practical measurement tasks, PIENet still provides a reasonable and verifiable uncertainty statement for the reported results, thereby supporting reliable decision-making in I&M applications.

When the predictive performances of different models are similar, the evaluation of uncertainty plays an essential role in assessing their reliability and distinguishing the metrological credibility of each method. The proposed PIENet provides more calibrated and physically consistent uncertainty estimates, thus offering a more reliable basis for comparison.

Although we have calibrated the uncertainty of the predictions through the loss function, there is a need in future work to improve the reliability of the model's uncertainty estimation by incorporating the actual characteristics of physical models. While the current focus is primarily on single-input-single-output systems, the framework can be extended to multiple-input–multiple-output systems by studying the coupled dynamics in multiple degree-of-freedom systems and managing the complexity of high-dimensional spaces. This would further enhance the applicability and generalizability of the model.

REFERENCES

- [1] P. da Silva Hack and C. S. ten Caten, "Measurement uncertainty: Literature review and research trends," *IEEE Trans. Instrum. Meas.*, vol. 61, no. 8, pp. 2116–2124, Aug. 2012.
- [2] N. Kusnandar, H. Firdaus, I. Supono, B. Utomo, I. Kasiyanto, and Q. Lailiyah, "Bibliometric review of measurement uncertainty: Research classification and future tendencies," *Measurement*, vol. 232, Jun. 2024, Art. no. 114636.
- [3] O. Vasilevskyi, V. Kucheruk, and I. P. Kurytnik, "An approach to the evaluation of dynamic uncertainty in measurement using non-statistical techniques," *Pomiary Automatyka Kontrola*, vol. 60, no. 11, pp. 997–1001, 2014.
- [4] Evaluation of Measurement Data-Guide to the Expression of Uncertainty in Measurement, Standard JCGM 100:2008, Int. Organ. Stand. Geneva, Switzerland, 2008, p. 134.
- [5] J. Wirandi, A. Lauber, and W. J. Kulesza, "Problem of applying modern uncertainty concepts to the measurement of instrument-specific parameters," *IEEE Trans. Instrum. Meas.*, vol. 55, no. 3, pp. 700–705, Jun. 2006.
- [6] S. Shirmohammadi and H. Al Osman, "Machine learning in measurement part 1: Error contribution and terminology confusion," *IEEE Instrum. Meas. Mag.*, vol. 24, no. 2, pp. 84–92, Apr. 2021.
- [7] J. Zhu, Z. Wang, X. Xia, and P. Li, "Approach for the evaluation of indirect measurement uncertainty based on neural networks," *Proc. SPIE*, vol. 5253, p. 303, Sep. 2003.
- [8] T. Mueller, M. Huber, and R. Schmitt, "Modelling complex measurement processes for measurement uncertainty determination," *Int. J. Quality Rel. Manage.*, vol. 37, no. 3, pp. 494–516, Mar. 2020.
- [9] C. Elster and A. Link, "Uncertainty evaluation for dynamic measurements modelled by a linear time-invariant system," *Metrologia*, vol. 45, no. 4, pp. 464–473, Aug. 2008.
- [10] S. Eichstädt, A. Link, P. Harris, and C. Elster, "Efficient implementation of a Monte Carlo method for uncertainty evaluation in dynamic measurements," *Metrologia*, vol. 49, no. 3, pp. 401–410, Jun. 2012.
- [11] L. Ye, X. Xia, and Z. Chang, "Evaluation of dynamic uncertainty of rolling bearing vibration performance," *Math. Problems Eng.*, vol. 2019, no. 1, Jan. 2019, Art. no. 2896046.
- [12] J. Dai, S. Adhikari, and M. Wen, "Uncertainty quantification and propagation in atomistic machine learning," *Rev. Chem. Eng.*, vol. 41, no. 4, pp. 333–357, May 2025.
- [13] H. Al Osman and S. Shirmohammadi, "Machine learning in measurement—Part 2: Uncertainty quantification," *IEEE Instrum. Meas. Mag.*, vol. 24, no. 3, pp. 23–27, May 2021.
- [14] J. Gawlikowski et al., "A survey of uncertainty in deep neural networks," *Artif. Intell. Rev.*, vol. 56, no. 1, pp. 1513–1589, 2023.
- [15] Y. Ding, W. Chen, R. Song, H. Li, C. Pan, and H. Xia, "Dynamic modeling and measurement uncertainty evaluation of the nonlinear piezoelectric impulse drive system with small samples," *IEEE Trans. Instrum. Meas.*, vol. 74, pp. 1–11, 2025.
- [16] W. Chen, H. Xia, R. Song, and C. Pan, "Dynamic modeling and performance evaluation of piezoelectric impact drive system based on neural network," *Meas. Sci. Technol.*, vol. 34, no. 10, Oct. 2023, Art. no. 105021.
- [17] C. Su, J. Tong, Y. Zhu, P. Cui, and F. Wang, "Network embedding in biomedical data science," *Briefings Bioinf.*, vol. 21, no. 1, pp. 182–197, Jan. 2020.
- [18] P. Rajendra, K. V. N. Murthy, A. Subbarao, and R. Boodh, "Use of ANN models in the prediction of meteorological data," *Model. Earth Syst. Environ.*, vol. 5, no. 3, pp. 1051–1058, Sep. 2019.
- [19] G. E. Karniadakis et al., "Physics-informed machine learning," *Nature Rev. Phys.*, vol. 3, no. 6, pp. 422–440, 2021.
- [20] S. Lin and Y. Chen, "Gradient-enhanced physics-informed neural networks based on transfer learning for inverse problems of the variable coefficient differential equations," *Phys. D, Nonlinear Phenomena*, vol. 459, Mar. 2024, Art. no. 134023.
- [21] A. Amini et al., "Deep evidential regression," in *Proc. Adv. Neural Inf. Process. Syst.*, vol. 33, 2020, pp. 14927–14937.
- [22] Y. Park, K. Gajamannage, D. I. Jayathilake, and E. M. Boltt, "Recurrent neural networks for dynamical systems: Applications to ordinary differential equations, collective motion, and hydrological modeling," 2022, *arXiv:2202.07022*.
- [23] R. Coral, C. A. Flesch, C. A. Penz, M. Roisenberg, and A. L. S. Pacheco, "A Monte Carlo-based method for assessing the measurement uncertainty in the training and use of artificial neural networks," *Metrol. Meas. Syst.*, vol. 23, no. 2, pp. 281–294, Jun. 2016.
- [24] N. Geneva and N. Zabaras, "Transformers for modeling physical systems," *Neural Netw.*, vol. 146, pp. 272–289, Feb. 2022.
- [25] L. Girin, S. Leglaive, X. Bie, J. Diard, T. Hueber, and X. Alameda-Pineda, "Dynamical variational autoencoders: A comprehensive review," 2020, *arXiv:2008.12595*.
- [26] A. Arzani, J.-X. Wang, and R. M. D'Souza, "Uncovering near-wall blood flow from sparse data with physics-informed neural networks," *Phys. Fluids*, vol. 33, no. 7, pp. 1–19, Jul. 2021.
- [27] S. Cai, C. Gray, and G. E. Karniadakis, "Physics-informed neural networks enhanced particle tracking velocimetry: An example for turbulent jet flow," *IEEE Trans. Instrum. Meas.*, vol. 73, pp. 1–9, 2024.
- [28] J. Liu, P. Borja, and C. D. Santina, "Physics-informed neural networks to model and control robots: A theoretical and experimental investigation," *Adv. Intell. Syst.*, vol. 6, no. 5, May 2024, Art. no. 2300385.
- [29] S. Shirmohammadi, "Measurement methodology: Visualizing uncertainty in machine learning-assisted measurements," *IEEE Instrum. Meas. Mag.*, vol. 26, no. 7, pp. 20–27, Oct. 2023.
- [30] X. Zhou, H. Liu, F. Pourpanah, T. Zeng, and X. Wang, "A survey on epistemic (model) uncertainty in supervised learning: Recent advances and applications," *Neurocomputing*, vol. 489, pp. 449–465, Jun. 2022.

- [31] S. Feng, C. Zuo, Y. Hu, Y. Li, and Q. Chen, "Deep-learning-based fringe-pattern analysis with uncertainty estimation," *Optica*, vol. 8, no. 12, pp. 1507–1510, Dec. 2021.
- [32] R. Song, H. Wang, H. Xia, J. Cheng, C. Li, and X. Chen, "Uncertainty quantification for deep learning-based remote photoplethysmography," *IEEE Trans. Instrum. Meas.*, vol. 72, pp. 1–12, 2023.
- [33] L. Hoffmann, I. Fortmeier, and C. Elster, "Uncertainty quantification by ensemble learning for computational optical form measurements," *Mach. Learn., Sci. Technol.*, vol. 2, no. 3, Sep. 2021, Art. no. 035030.
- [34] C. Chen et al., "U²D²PCB: Uncertainty-aware unsupervised defect detection on PCB images using reconstructive and discriminative models," *IEEE Trans. Instrum. Meas.*, vol. 73, pp. 1–10, 2024.
- [35] B. Lakshminarayanan, A. Pritzel, and C. Blundell, "Simple and scalable predictive uncertainty estimation using deep ensembles," in *Proc. Adv. Neural Inf. Process. Syst.*, 2017, pp. 6402–6413.
- [36] R. Rahaman, "Uncertainty quantification and deep ensembles," in *Proc. Adv. Neural Inf. Process. Syst.*, vol. 34, 2021, pp. 20063–20075.
- [37] H. Siong Tan, K. Wang, and R. McBeth, "Evidential physics-informed neural networks," 2025, *arXiv:2501.15908*.
- [38] Y. J. Kai, E. de Conto, and A. Easwaran, "Quantifying uncertainty in physics-informed neural networks," in *Proc. AI4X Int. Conf.*, 2025, pp. 8–11.
- [39] S. H. Strogatz, *Nonlinear Dynamics and Chaos: With Applications to Physics, Biology, Chemistry, and Engineering*. Chapman & Hall/CRC, 2024.
- [40] T. Wigren and J. Schoukens, "Data for benchmarking in nonlinear system identification," Dept. Inf. Technol., Uppsala, Sweden, Tech. Rep., Mar. 2013, vol. 6. [Online]. Available: <http://www.it.uu.se/research/publications/reports/2013-006/SNLA80mVZipped.zip>
- [41] M.-G. Hu, C.-L. Pan, J.-H. Wu, A.-H. Feng, H. Jiang, and H.-J. Xia, "Design of a parallel linear platform based on piezoelectric inertial drive mechanism," in *Proc. 15th Symp. Piezoelectricity, Acoustic Waves Device Appl. (SPAUDA)*, Apr. 2021, pp. 44–48.
- [42] R. Nayek, R. Fuentes, K. Worden, and E. J. Cross, "On spike-and-slab priors for Bayesian equation discovery of nonlinear dynamical systems via sparse linear regression," *Mech. Syst. Signal Process.*, vol. 161, Dec. 2021, Art. no. 107986.
- [43] Y. Hou et al., "An efficient deconvolution method for automatic detection of bearing localized defect based on Bayesian optimization," *IEEE Trans. Instrum. Meas.*, vol. 73, pp. 1–15, 2024.
- [44] H. Wang, L. Meng, and Y. Qu, "Bootstrap-based multitask deep learning method for uncertainty estimation and correction in TSOM," *IEEE Trans. Instrum. Meas.*, vol. 74, pp. 1–10, 2025.
- [45] S. H. Tan, K. Wang, and R. Mcbeth, "Uncertainty-error correlations in evidential deep learning models for biomedical segmentation," in *Proc. Int. Conf. Technol. Appl. Artif. Intell.* Singapore: Springer, 2024, pp. 91–105.
- [46] D. Matzke et al., "Bayesian inference for correlations in the presence of measurement error and estimation uncertainty," *Collabra: Psychol.*, vol. 3, no. 1, Jan. 2017, doi: [10.1525/collabra.78](https://doi.org/10.1525/collabra.78).



Wenhao Chen was born in Anhui, China, in 1998. He received the B.S. degree from Anhui University, Hefei, China, in 2021. He is currently pursuing the Ph.D. degree with Hefei University of Technology, Hefei.

He mainly engaged in research on neural network-based measurement uncertainty evaluation of dynamic systems and neural network modeling of dynamic measurement systems.



Yinye Ding was born in Tongling, Anhui, China, in 1999. She received the bachelor's of science degree from Anhui Normal University, Wuhu, China, in 2019. She is currently pursuing the Ph.D. degree with Hefei University of Technology, Hefei, China.

She is mainly engaged in the theoretical study of measurement uncertainty evaluation and the analysis of small-sample measurement data.



Rencheng Song (Senior Member, IEEE) is a Professor with the School of Instrument Science and Opto-Electronics Engineering, Hefei University of Technology, Hefei, China. His current research interests include human-centered intelligent perception and natural human-machine interaction.



Chengliang Pan was born in Wuhu, Anhui, China, in 1983. He is currently a Professor with the School of Instrument Science and Opto-Electronics Engineering, Hefei University of Technology, Hefei, China. His research interests include precision instruments and machinery, advanced sensors and actuators, and their applications in industries.



Huining Zhao is an Associate Professor with the School of Instrument Science and Opto-Electronics Engineering, Hefei University of Technology, Hefei, China. His main research areas are instrument accuracy theory, coordinate measurement technology, and precision instrument design.



Hongli Li received the Ph.D. degree in test metrology technology and instruments from Hefei University of Technology, Hefei, China, in 2015.

She is an Associate Professor with the School of Instrument Science and Opto-Electronics Engineering, Hefei University of Technology. Her research interests include modern precision theory and application, measurement uncertainty theory and application.



Haojie Xia (Member, IEEE) was born in Suzhou, Anhui, China, in 1979. He received the Ph.D. degree from Hefei University of Technology, Hefei, China, in 2006.

He was a Visiting Scholar with German Federal Institute of Physics (PTB), Braunschweig, Germany, in 2015. He is currently a Professor with Hefei University of Technology. He mainly engages in research work in fields such as optoelectronic precision measurement technology, micro/nano measurement and control systems, instrument accuracy theory, and precision instrument design.